Towards automatic transcatheter heart valve parametrisation on X-ray sequences

1st Alma Vivas Lago
University of Vigo
Vigo, Spain
alvivas@alumnos.uvigo.es

***Abstract*—The durability and potential modes of failure for heart implants, particularly next-generation tissue-engineered valves such as those utilized in transcatheter aortic valve (TAV) procedures, are not well understood. This is partly due to the limitations of current methods for measuring the actual deformations that the bioprosthesis experiences during a patient's cardiac cycle, which obstructs accurate evaluation of the implant's performance. To address these issues, a novel computational framework has been proposed. The framework utilizes x-ray images as input and converts them into a patient-specific, discretized geometric model. The model captures the mechanical deformations and temporal changes in valve geometry that occur during the cardiac cycle. The system performance is evaluated by comparing the properties of an user-generated geometric model to the output generated by the algorithm. The evaluation encompasses classical regression error metrics, degree of completeness and shape similarity. Results from 17 patients demonstrated an index of completeness of 87.9% and normalized Hausdorff shape similarity score of 88.5%. Furthermore, the framework allows for the analysis of the temporal evolution of a transcatheter heart valve (THV) model, providing insight into its contractibility. This indirectly confirms the hypothesis that the THV oscillation remains closely synchronized with an electrocardiogram (ECG) during the heart beat. In conclusion, the framework holds promise as a tool for monitoring the degradation of the prosthesis in vivo, and has the potential to advance our understanding of THV performance and lead to the development of more durable bioprosthetic heart valves.**

***Index Terms*—Image processing, transcatheter heart valves, bioprosthetic heart valves, finite element analysis.**

I. Introduction

Transcatheter aortic valve implantation (TAVI) has established itself as a globally recognized standard surgical treatment for patients with severe aortic stenosis and high surgical risk [1]. As the number of patients treated for aortic valve disease continues to rise, the indication criteria have broadened to encompass younger patient populations with lower risk profiles [2], [3].

Given the growing demand for TAVI, there is a pressing need to develop innovative strategies for evaluating and optimizing device design, with an emphasis on long-term durability [3]–[6]. Fatigue-induced deterioration is a key factor affecting the longevity of valves, with inconsistent results from current studies [3], [5], [7] .

In order to address this challenge, a computational framework is proposed to accurately gather measurements from in vivo Transcatheter Heart Valve (THV) models. This system features a tool that captures the temporal evolution of valve geometry based on personalized data during the cardiac cycle.

II. Contextual Background

A. Aortic Valve Replacement: an overview

Aortic valve replacement is a surgical procedure that involves removing a damaged or diseased aortic valve and replacing it with a new valve. Traditionally, surgical aortic valve replacement (SAVR) involves open heart surgery and requires a sternotomy. Recently, a minimally invasive alternative known as transcatheter aortic valve implantation (TAVI) has been developed [8]–[10]. SAVR is a traditional surgical approach that involves median sternotomy and cardiopulmonary bypass. The patient's chest is opened and the heart is stopped so that the damaged valve can be removed and replaced. During the procedure, the defective aortic valve is removed and replaced with a prosthetic valve. The prosthetic valve is sutured into position and reinforced with annuloplasty rings to guarantee accurate positioning. SAVR is a highly successful procedure with a low incidence of valve failure and long-term durability. However, it is an invasive procedure that necessitates general anesthesia, incurs a prolonged recovery period, and carries a higher risk of complications such as stroke and bleeding [8], [10]–[13].

TAVI, in contrast, is a minimally invasive procedure that does not require open heart surgery. The prosthetic valve is delivered to the site of the defective valve via a catheter and positioned in place using various deployment techniques, including balloon-expandable or self-expanding valve technology. TAVI is characterized by a shorter recovery time, lower invasiveness, and lower risk of complications in comparison to SAVR. Nonetheless, the long-term durability and efficacy of TAVI remains subject to evaluation and may be influenced by patient-specific factors such as anatomy, comorbidities, and age [8], [12]–[17].

Both SAVR and TAVI are effective options for aortic valve replacement, each with its unique advantages and disadvantages. The choice between the two procedures will depend on the patient's overall health and specific medical needs [2], [6].

B. Trends and challenges in TAVI Biomechanical analysis

The study of TAVI biomechanics remains a pivotal area of investigation within the realm of computational modeling, as it provides a highly effective means of determining the long-term durability of valve devices [18]. Despite recent advancements, there exist several trends and challenges that must be addressed in order to fully realize the potential of computational modeling in clinical applications [19].

One key challenge facing the study of TAVI biomechanics is the limited availability of in vivo data. This often results in researchers relying on in vitro data or idealized models to represent valve behavior, which detracts from the accuracy of simulations as the real-world behavior of the valve within the living heart cannot be accurately captured [20], [21].

The increasing utilization of Finite Element Analysis (FEA) for TAVI biomechanics has become a prominent trend in the field. FEA offers a powerful simulation tool for the examination of valve mechanics and dynamic behavior [7], [22], [23]. However, it is crucial to consider FEA limitations, as the simulations accuracy is dependent on the input data quality and the validity of assumptions made within the model.

Recent studies have aimed to provide high-fidelity simulations that are patient-specific, yet the only patient-specific data that is typically provided are anatomical models and not bioprosthesis parameters [20], [22], [24], [25].

To overcome these challenges, there is a growing effort to develop new strategies for TAVI biomechanics assessment that will address the limitations of FEA and provide a more accurate representation of the real-world behavior of the valve. The use of high-precision automated measurement tools has emerged as a highly promising approach, as it offers a non-invasive method of evaluating THV devices in vivo.

In conclusion, the study of TAVI biomechanics presents a wealth of opportunities and challenges that must be addressed in order to fully realize the potential of computational modeling in clinical applications. The development of innovative strategies for TAVI biomechanics assessment represents a promising direction for the advancement of heart simulations and offers a valuable opportunity for future research in the field [26].

III. Algorithmic approach

The novel computational framework is a twofold system: detection scheme and measurement extraction pipeline.

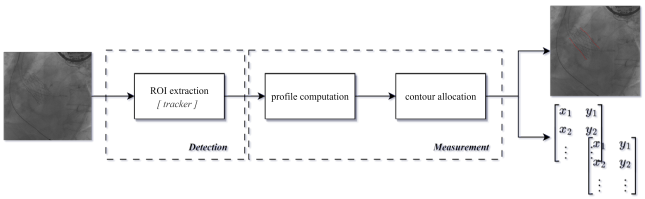

Fig. 1. Ilustration of the two-fold computational framework for valve geometric analysis. The framework comprises of two stages: detection and measurement extraction. The detection stage is comprised of a single block referred to as the region of interest extraction, which is responsible for the identification and tracking of the spatiotemporal coherence of the region of interest. The measurement extraction stage comprises of two blocks, profile computation, and contour allocation. This stage generates a visual representation of the geometrically parametrized valve, as well as a set of arrays in the vectorized form of the contours.

A. Detection scheme

The initial step involves downscaling all frames by half to reduce processing time. A specialized skeletonization technique is then utilized to extract the structure of interest through the following steps: histogram equalization, application of the Meijering neurite filter, and outlier removal via a non-linear order-static filter. These processes are repeated for different kernel sizes and standard deviations, resulting in multiple images that are merged using a logical OR operator.

Next, a gabor filter bank is applied to generate a clear contour of the structure. The range of theta values corresponding to the structure's orientation (i.e., fourth quadrant) is selected, and a convolution is performed at various frequencies. It should be noted that some distortion may occur due to the loss of spatial information. A cleaning process is then performed through connected component analysis to remove blobs that do not exceed a certain threshold.

A gaussian low-pass filter, Otsu's thresholding, and a fill-in function (invading the complement of the shapes) are applied to the skeletonized image. The resulting binary image undergoes connected component analysis, with the frequency of each component being counted. Only the highest component is selected, with the rest being removed (e.g., artifacts such as a catheter section).

The process then branches into two paths (for clear visualization, see section C flowchart). The first path involves extracting references from the first frames. This strategy involves stacking all images into a single three-dimensional array from which a probability map is calculated by summing up the spatially common pixels. For each uncertainty level, a topological structural analysis of images is performed via boundary tracking to extract the minimum area rectangle.

A scoring system has been developed to evaluate the most likely candidate region size based on the aspect ratio, solidity, the number of non-zero pixels, and uncertainty level. Exploiting prior knowledge about the stent dimensions (provided by the manufacturer), the ideal aspect ratio is used as a member of the equation, with the core scoring method being expressed in equation 1.

$$score = \frac{aspect\ ratio}{ideal\ aspect\ ratio} + solidity + \frac{uncertanty\ level}{10} \quad (1)$$

The process of determining the most likely candidate region size involves the application of THE scoring system. Figure 2 provides a visual representation of how these factors influence the final determination of the minimum area rectangle.

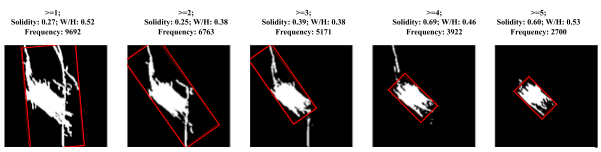

Fig. 2. Evaluation of the most likely candidate region size based on uncertainty level, aspect ratio, solidity, and non-zero frequency count. The minimum area rectangle is determined through boundary tracking of topological structural analysis of images at various uncertainty levels.

The second path involves searching for the ROI by means of the external contour, with topological structural analysis being used to fit a bounding box that isolates the structure of interest. Based on the local displacement and variation with respect to the reference, some switch case corrections might be activated, suggesting an alternative location for the device. In such cases, information from the previous frame is reused or the initial reference extent and aspect is forced. Finally, the original image size is recovered and the ROI is scaled up.

B. Measurement pipeline

The opening step entails denoising the x-ray frame's region of interest (ROI) via gradient descent scheme with the L1 norm as the resolution routine. The identical skeletonization-like technique utilized previously followed by a chain of morphological dilation/erosion and masking operations form the basis is recycled as a preprocessing stage.

To convert pixel values into a set of two vectors that model the contours, an intensity-based profiler is constructed. The minimum enclosing rectangle is used to define the location, limits, and trajectory, with the upper edge serving to bound location and limits and the trajectory being expressed through the slope of the side rectangle edges (solved through a linear matrix equation).

The vector lines are mapped through the rasterization of non-zero pixels, with a loss of precision in materializing the unit of measurement (i.e., the pixel). Border allocation then ensues by analyzing the outermost values within each profiled row. Edges are iteratively filtered through polynomial fitting, interpolated using a spline function, and a smoothed Savitzky-Golay filter is applied.

C. Real-time system integration

In this subsection, the design and implementation of the real-time system integration is presented. The underlying concept behind this type of integration is to simulate a realistic acquisition scenario and design the real-time system to be tested in it. It is implemented as a consumer-producer fashion, where the producer simulates a camera feed and generates images at a specified frame rate by employing an sleep function. The images are stored in a queue, which serves as a buffer, and the consumer retrieves the images with the utmost efficiency. The processed images are then passed on to the system for analysis. The system comprises two subsystems, one of which is dedicated to stabilization, which involves accurately estimating the dimensions and orientation of the region of interest, while the other subsystem sequentially processes each frame through the main pipeline.

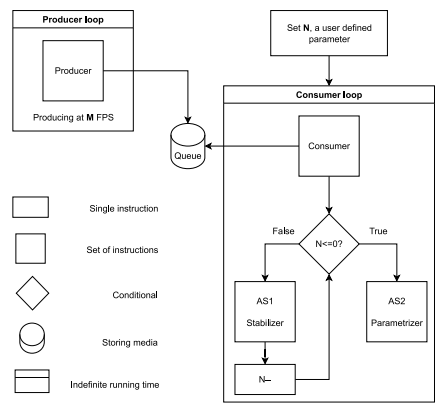

Fig. 3. This flowchart shows how the developed system should fit inside the classical producer/consumer paradigm. The *producer* by the clinical standard protocol is set to simulate a feed of images at M FPS. The *consumer* will then feed the automatic implant parametrisation system created. This system will switch execution between *AS1* and *AS2* based on N, an user input that determines the number of frames needed for the system stabilization.

IV. Experimental Evaluation

This section delves into the evaluation of the system's performance through the use of real-life clinical case data. The methodology and outcomes are presented systematically, encompassing data characterization, metric choice, and result analysis. The evaluation is organized into four sub-sections: clinical cases, Transcatheter Heart Valve model, validation methodology, and results.

A. Clinical cases

This study analyzed 17 patients diagnosed with severe aortic stenosis who underwent TAVI procedures at the Department of Cardiology of Álvaro Cunqueiro Hospital in Vigo, Spain. The data was collected between June 2019 and January 2020 and involved patients with Allegra THV implants of varying sizes (23 mm, 27 mm, or 31 mm). The study received ethical approval and all patients provided informed consent to ensure the safe and responsible use of their data.

TABLE I
Details of the data used in the study.

N. of patients	17
N. of sequences	68
N. total frames	3,804
N. of frames per sequences	25 - 100
Image size	512 × 512 *pixels*
Resolution	8 *bits*
Pixel spacing	0.34 *mm*
Fps	15 and 25
Acquisition technique	Cine angiography
Equipment	AlluraClarity with ClarityIQ

The data collected for this study involved a different of number of x-ray sequences, captured from each patient in different projections, in accordance with the local protocol at the participating site. Additionally, at least one complete heartbeat was guaranteed in each sequence. Therefore, providing a realistic depiction of a THV model in use and its operating conditions. Table IV-A provides additional details of the data used in this study. A sample of the dataset can be seen in Fig. 4.

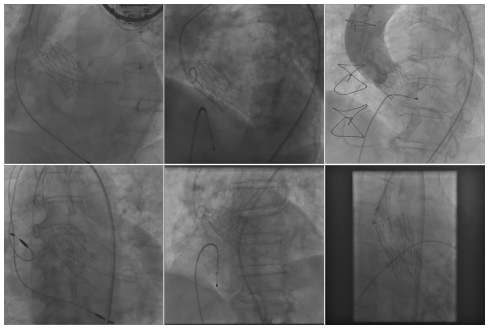

Fig. 4. Clinical Data Representative Subset: A visual representation of the acquired x-ray angiography images in varying conditions, showcasing the realistic depiction of a TAV model in use.

B. Transcatheter Heart Valve model

The Allegra THV (New Valve Technology AG, Muri, Switzerland) a features a nitinol self-expandable stent frame and bovine pericardium leaflets. There are six radiopaque gold markers placed at the valve plane level as an aid to the operator in positioning. The valve's morphology includes the outflow diameter , the commissural outflow diameter, and the inflow diameter, shown in Fig. 5 .

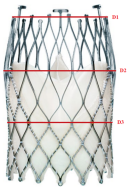

Fig. 5. Allegra TVH key features. Outflow diameter (Stent tip), D1; Commissural outflow diameter (maximum dimension), D2; Inflow diameter (minimum dimension), D3.

C. Metrics and validation methodology

In addition to standard error metrics, the system's performance was also evaluated through the consideration of pixel presence or absence, as well as shape similarity.

RMSE (Root Mean Squared Error) and MAE (Mean Absolute Error) are common metrics used in regression problems to evaluate the performance of prediction models. They measure the difference between the predicted values and the true values, with RMSE taking into account the magnitude of the error, and MAE focusing on the average magnitude. When applied to predictions in pixels, they can be interpreted as the average difference and average magnitude of the error, respectively, between the true and predicted values.

Completeness metrics are also used to evaluate the presence or absence of pixels. They are expressed as a percentage of the total number of pixels that should be present, and aim to provide a numerical summary of the degree of completeness. This allows for comparisons between models or changes in quality over time.

In order to determine a final metric for the completeness of the structure, a weighted average formula is used. This formula takes into account the relative significance of the start and end portions of the structure, and is based on the measures of start extra (SE), start missing (SM), end extra (EE), and end missing (EM). The formula for the index of completeness is expressed in 2.

$$IC = 1 - ((W_{start} * \frac{SE + SM}{2}) + (W_{end} * \frac{EE + EM}{2})) \quad (2)$$

Where IC is the index of completeness, W_{start} and W_{end} are the respective weights assigned to the start and end portions of the structure. The resulting value of IC ranges from 0 to 1, with 1 indicating a fully complete structure. It is important to note that W_{start} and W_{end} must sum up to 1.

The Hausdorff distance is a well-established metric in the biomedical field for evaluating the similarity between two sets of points, such as shapes. This measurement is calculated by determining the maximum distance between any point in one shape and its nearest point in the other shape. A smaller Hausdorff distance indicates a greater degree of similarity between the two shapes. The computation involves centering both shapes, then finding the maximum distance between each point in one shape and its closest point in the other shape. The final result is the largest of these distances, providing a comprehensive evaluation of the similarity between the two shapes. In the following analysis, the Hausdorff similarity score will be referred to as HSS.

The evaluation methodology involves using an annotation tool to characterize the contour of the structure based on its morphological features. The inflection points were identified and interpolated using spline functions, then smoothed using a Savitzky-Golay filter to minimize any inaccuracies due to discretization. This process generates a high-fidelity representation of the morphological characteristics of the structure, providing a comprehensive evaluation of its performance. The process of annotation and its implementation is illustrated in the accompanying figure, Fig. 6.

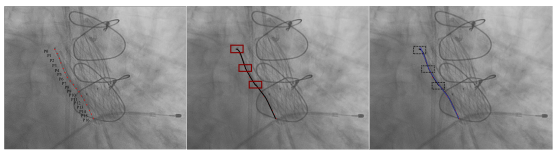

Fig. 6. An illustration of the user-generated geometric model evaluation methodology, consisting of three steps. Step 1 depicts the discretized geometric model, which is represented by 16 red keypoints. Step 2 is the interpolated spline, shown in black, connecting the selected anchors (red keypoints) to reduce discretization or noise-related artifacts (indicated by red rectangles). Step 3 shows the final smooth version, produced using the Savitzky-Golay filter (represented in blue), that significantly reduces inaccuracies, as demonstrated by the black dashed rectangles. The combination of the annotation and implementation process results in a comprehensive evaluation of the structure's morphological characteristics and a high-fidelity representation of its performance.

The evaluation of the THV system was focused on its ability to analyze the changing geometry of the valve over time, with an emphasis on long-term durability. The manufacturer's claimed geometrical features (illustrated in Fig. 5) were used in the analysis, and the diameters D2 and D3 were calculated as the longest and shortest distances between two curves, respectively. However, the asymmetrical T-like structure of D1 posed a challenge, which was addressed by fitting a line to the shorter side, calculating the middle plane, and, if necessary, intersecting the problematic border. The prosthesis's contractibility, which is a factor in its degradation, was analyzed by measuring and plotting the diameters. The starting integrity of the stent tip is particularly crucial for this THV model. Therefore, as described in equation 2, the weight for the start portion should be higher compared to the end portion, and these weights can be adjusted based on the specific needs of the application.

D. Results

In this section, the performance of the proposed method is quantitatively evaluated through a comprehensive set of validation metrics. As an standard for this type of problem, MAE and RMSE values are expressed in pixels. Lower values of these metrics indicate better performance and greater accuracy of the model. The completeness metrics, are represented by the extra and missing length of the obtained model relative to the ground truth (GT) total segment length. The maximum value is 1, which occurs when either the extra pixels are the same length as the entire segment or the entire segment is missing, representing the worst-case scenario. A value of 0 means there is no offset of missing pixels, and the closer the value is to zero, the more precise the results.

Table II shows the overall assessment of the study. The index of completeness (IC) weights, W_{start} and W_{end}, are assigned to 0.7 and 0.3, respectively. In order to normalize the Hausdorff similarity score (HSS) is divided by the calculated maximum possible distance between the two sets of keypoints. The resulting value is a unit less similarity score that can be compared between different shapes, eliminating the influence of scale on the similarity score.

TABLE II
OVERALL ASSESSMENT: PARAMETRIZATION

IC	Normalized HSS
0.88 ± 0.1	0.89 ± 0.28

Table III displays the overall results of the 17 patients analyzed in this study. The terms SE, SM, EE, and EM refer to the start and end of the curve and whether there are extra or missing pixels in the segmentation. SE stands for start extra, SM stands for start missing, EE stands for end extra, and EM stands for end missing.

TABLE III
OVERALL DETAIL METRICS: PARAMETRIZATION

MAE	RMSE.	SE/GT	SM/GT	EE/GT	EM/GT
8.59 ± 7.13	9.20 ± 8.56	0.08 ± 0.06	0.16 ± 0.10	0.18± 0.17	0.07± 0.05

Table III shows that on average, the model has a MAE of 8.59 pixels and a RMSE of 9.20 pixels. The standard deviations are 7.13 pixels and 8.56 pixels, respectively. Table also reveals that the beginning of the sequence has, on average, 16% of the segment missing with a standard deviation of 10%, and 8% of the segment is extra, with a standard deviation of 6%. This can be attributed to the hindrance of the aortic root contrast in clearly identifying the valve. The end part of the structure has an average of 18% of the segment missing and 7% extra, with standard deviations of 17% and 5% respectively, due to the increased difficulty in accurately segmenting this part of the structure. A deeper insight into these limitations is the motivates Fig. 7. It presents the some challenges facing the THV angiography recognition process and identifies the main structures of the human body as potential sources of failure.

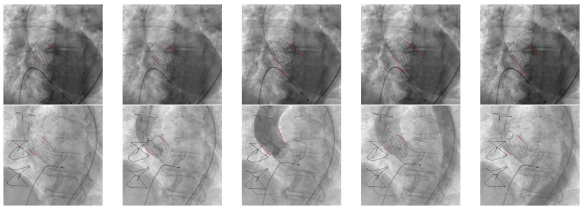

Fig. 7. Identified method's failure modes due to contrast and overlapping with human body internals. Two sets of frames highlighting the failure modes of the method are presented. The first set depicts the failure of the method due to several complications in the image: in the whole set of frames the outer contours towards the top extrema of the piece have low contrast when compared with the background, which makes it difficult to identify them; the catheter when close to the valve sometimes may get misidentified, as it can be seen in the third and fourth frame; it can also be observed how the patient vertebral column interferes with the recognition of the valve when in superposition. The second set, depicts a slightly different failure scenario but with same root causes: it can be observed how the contrast between the background plays a huge role in being able to recognize the tips of the piece, as it can be seen throughout the whole sequence; being the catheter in superposition with bottom of the vale may compound the inability to recognize its lower borders; it can be observed how the aortic root can be misclassified as being part of the piece when placed one above the other. This last cause, identifies the human body major structures as potential sources of failures.

Table IV presents a summary of the parametrization results for each patient and sequence. The results are displayed in bold style to emphasize the best and worst performance for each metric. The worst performance is further highlighted in red for visual emphasis. These results provide a comprehensive overview of the performance of the proposed method and highlight areas for improvement in future work.

TABLE IV
VALIDATION METRICS PARAMETRIZATION

Patient	N. Seq.	MAE	RMSE	Extra/GT	Missing/GT
A	3	**5.21 ± 2.59**	**5.56 ± 2.76**	0.22 ± 0.12	0.09 ± 0.02
B	2	5.93 ± 4.16	6.19 ± 4.22	0.12 ± 0.04	0.08 ± 0.02
C	1	6.89 ± 1.97	7.15 ± 1.94	0.12 ± 0.02	0.07 ± 0.01
D	3	6.33 ± 3.19	6.69 ± 3.43	0.08 ± 0.04	0.06 ± 0.02
E	4	6.90 ± 3.38	7.19 ± 3.48	0.12 ± 0.04	0.09 ± 0.01
F	4	6.86 ± 2.93	7.37 ± 3.15	0.14 ± 0.05	0.07 ± 0.02
G	3	18.34 ± 13.37	20.97 ± 16.28	0.24 ± 0.08	0.07 ± 0.01
H	2	27.91 ± 22.73	34.93 ± 29.39	0.35 ± 0.14	0.06 ± 0.00
I	4	7.70 ± 3.20	8.15 ± 3.32	0.11 ± 0.02	0.08 ± 0.03
J	3	12.27 ± 6.74	12.86 ± 6.90	0.24 ± 0.11	nan ± nan
K	4	8.43 ± 3.49	8.60 ± 3.54	**0.08 ± 0.01**	**0.05 ± 0.03**
L	2	7.32 ± 2.23	7.50 ± 2.25	0.11 ± 0.02	0.07 ± 0.05
M	4	6.88 ± 3.82	7.13 ± 3.85	0.11 ± 0.01	0.07 ± 0.01
N	4	8.34 ± 4.09	8.66 ± 4.14	0.16 ± 0.05	0.06 ± 0.01
O	3	9.25 ± 4.20	9.69 ± 4.30	0.19 ± 0.04	0.06 ± 0.00
P	4	6.97 ± 3.23	7.21 ± 3.27	0.09 ± 0.03	0.09 ± 0.04
Q	3	6.93 ± 2.50	7.28 ± 2.62	0.20 ± 0.04	0.10 ± 0.02

Supplementary results of the study are presented in appendix A. This section provides a visual representation of THV device geometries for each validated target, offering further insight into the limitations and scope of the computational framework used in the study. The results of the evaluation criteria are also detailed to support the conclusions and findings of the study.

Temporal evolution of valve geometry. The following graph (Fig. 8) showcases the oscillation of D1, D2, and D3 in the THV model. The detection of periodicity in the THV model's displacement signals implies a potential synchronization with either the electrocardiogram (ECG) or blood pressure (BP) cycles. It is important to recognize that while periodicity may suggest synchronization, it is not conclusive. To strengthen the confidence in this synchronization, cross-correlation analysis between the displacement signals and the ECG and BP signals must be performed, demonstrating a prominent peak at a lag consistent with the cardiac cycle period. Furthermore, the synchronization of the sampling rates of the signals and proper preprocessing and filtering to eliminate any confounding factors should be ensured. Therefore, a comprehensive analysis of the signals, taking into account various factors, is crucial for a meaningful interpretation of the results.

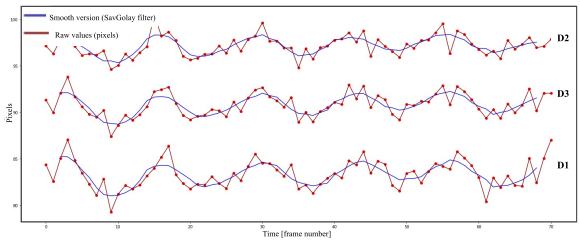

Fig. 8. Temporal evolution of THV model segments: demonstrating the oscillation of D1, D2, and D3 in relation to potential synchronization with ECG and BP Signals. The figure depicts the temporal evolution of the valve geometry in a THV model. The oscillation of three segments, D1, D2, and D3, are shown in the figure. The red points represent the raw data, while the blue line represents the smoothed version of the data obtained through the application of a Savitzky-Golay filter. The purpose of the filter is to remove any noise present in the raw data and reveal the underlying trend in the signal. The detection of periodicity in the THV model's displacement signals suggests a potential synchronization with either the electrocardiogram or blood pressure cycles. This analysis aims to provide insights into the deterioration of the valve by studying the oscillations in the THV model segments over time.

In the other hand, the process of evaluating the parameters involved in the analysis of a cardiovascular signal requires careful consideration of various factors. After thoroughly examining multiple sequences of the signal, it was determined that some sequences appeared appropriate for further analysis based on visual inspection. However, due to the inherent ambiguities and complexities associated with these sequences, it was ultimately decided to abstain from using them in order to avoid any potential sources of bias in the results. Given the nuanced relationship between the period of a cardiovascular signal and contractility stress, which can be influenced by factors such as the stage of the cardiac cycle, underlying pathophysiology, and the presence of other cardiovascular conditions, it was deemed necessary to take a cautious approach to data interpretation.

The study and characterization of such signals is beyond the scope of the presetned analysis. More information from different perspectives can be found in [27]–[29].

V. Conclusion

The objective of this study has been accomplished within a tolerable degree of accuracy. The results offer a glimpse into the reliability and accuracy of the tool, but also reveal limitations that require further attention. Despite these limitations, the temporal evolution of valve geometry provides intriguing insights into the harmony between prosthesis behavior and heart beat. It is imperative to further investigate the limitations and potential avenues for improvement to create a more robust evaluation and monitoring tool. Additionally, a more comprehensive analysis of larger clinical datasets is necessary to effectively monitor patient progression and enhance the classification system for device implantation, leading to improved procedural planning.

VI. Future work

The ability to achieve higher precision can be attributed to the utilization of ad hoc parameters that are selected post-empirical trials. Accordingly, the utilization of a branch-based distinction approach, supported by common scene features, holds the potential to yield favorable results.

Furthermore, the use of an intensity-based approach for selection, as opposed to key point detection, is particularly noteworthy due to its THV model agnosticism [30]. This property presents a unique opportunity to evaluate the framework's efficacy in a broader range of THV models. Given the need to address the complex and varied demands of various implant models, such an evaluation is essential to determine the generalizability and potential applicability in a wider context.

Future work for this project includes the unavoidable extension to 3D reconstruction, as 2D projections are incomplete. Ongoing efforts are being made to optimize state-of-the-art networks, such as NeRF [31] and its derived models, through exploration of different parameters and strategies. Traditional techniques such as structure for motion, [32], have also been explored [33]. While 3D reconstruction is still in its early stages for THV models, there is potential for valuable results if a morphing between these models and the ones introduced in this paper occurs.

Limitations of Python, the native prototyping language use to create the presented framework, for real-time implementation also pose a challenge in this study. Although the same methods were implemented in C++20, the lack of analogous functions in the language sometimes led to difficulties in finding the correct parameters for unfamiliar functions. As a result, the system, while able to provide real-time performance, required more time to optimize the parameters and ensure the correct functioning of the methods. Despite these limitations, the use of C++20 as the programming language was still deemed necessary for the real-time implementation of the system. Nevertheless, the ongoing effort to optimize and fine-tune the system will continue in the future.

References

[1] R. A. Nishimura, C. M. Otto, R. O. Bonow, B. A. Carabello, J. P. Erwin III, L. A. Fleisher, H. Jneid, M. J. Mack, C. J. McLeod, P. T. O'Gara *et al.*, "2017 aha/acc focused update of the 2014 aha/acc guideline for the management of patients with valvular heart disease: a report of the american college of cardiology/american heart association task force on clinical practice guidelines," *Circulation*, vol. 135, no. 25, pp. e1159–e1195, 2017.

[2] V.-. W. Committee, P. Généreux, N. Piazza, M. C. Alu, T. Nazif, R. T. Hahn, P. Pibarot, J. J. Bax, J. A. Leipsic, P. Blanke *et al.*, "Valve academic research consortium 3: updated endpoint definitions for aortic valve clinical research," *European heart journal*, vol. 42, no. 19, pp. 1825–1857, 2021.

[3] I. Richter, H. Thiele, and M. Abdel-Wahab, "Durability of transcatheter heart valves: standardized definitions and available data," *Journal of Clinical Medicine*, vol. 10, no. 18, p. 4180, 2021.

[4] J. Rodés-Cabau, "Transcatheter aortic valve implantation: current and future approaches," *Nature Reviews Cardiology*, vol. 9, no. 1, pp. 15–29, 2012.

[5] M. Arsalan and T. Walther, "Durability of prostheses for transcatheter aortic valve implantation," *Nature Reviews Cardiology*, vol. 13, no. 6, pp. 360–367, 2016.

[6] R. Puri, C. Chamandi, T. Rodriguez-Gabella, and J. Rodés-Cabau, "Future of transcatheter aortic valve implantation—evolving clinical indications," *Nature Reviews Cardiology*, vol. 15, no. 1, pp. 57–65, 2018.

[7] C. Martin and W. Sun, "Comparison of transcatheter aortic valve and surgical bioprosthetic valve durability: a fatigue simulation study," *Journal of biomechanics*, vol. 48, no. 12, pp. 3026–3034, 2015.

[8] J. Dominik and P. Zacek, *Heart valve surgery: an illustrated guide*. Springer Science & Business Media, 2010.

[9] P. A. Iaizzo, *Handbook of cardiac anatomy, physiology, and devices*. Springer Science & Business Media, 2010.

[10] S. R. Hardin and R. Kaplow, *Cardiac surgery essentials for critical care nursing*. Jones & Bartlett Learning, 2019.

[11] K. Maganti, V. H. Rigolin, M. E. Sarano, and R. O. Bonow, "Valvular heart disease: diagnosis and management," in *Mayo Clinic Proceedings*, vol. 85, no. 5. Elsevier, 2010, pp. 483–500.

[12] C. Cao, S. C. Ang, P. Indraratna, C. Manganas, P. Bannon, D. Black, D. Tian, and T. D. Yan, "Systematic review and meta-analysis of transcatheter aortic valve implantation versus surgical aortic valve replacement for severe aortic stenosis," *Annals of cardiothoracic surgery*, vol. 2, no. 1, p. 10, 2013.

[13] E. M. Antman, *Cardiovascular Therapeutics E-Book: A Companion to Braunwald's Heart Disease*. Elsevier Health Sciences, 2012.

[14] A. J. Nelson, N. J. Montarello, C. S. Cosgrove, R. L. Roberts-Thomson, S. Delacroix, R. G. Chokka, J. K. Montarello, and S. G. Worthley, "Transcatheter aortic valve implantation: a new standard of care," *Medical Journal of Australia*, vol. 209, no. 3, pp. 136–141, 2018.

[15] A. C. Watkins, A. Gupta, B. P. Griffith *et al.*, *Transcatheter Aortic Valve Replacement: A How-to Guide for Cardiologists and Cardiac Surgeons*. Springer, 2018.

[16] T. K. Rosengart, T. Feldman, M. A. Borger, T. A. Vassiliades Jr, A. M. Gillinov, K. J. Hoercher, A. Vahanian, R. O. Bonow, and W. O'Neill, "Percutaneous and minimally invasive valve procedures: a scientific statement from the american heart association council on cardiovascular surgery and anesthesia, council on clinical cardiology, functional genomics and translational biology interdisciplinary working group, and quality of care and outcomes research interdisciplinary working group," *Circulation*, vol. 117, no. 13, pp. 1750–1767, 2008.

[17] K. Steblovnik and M. Bunc, "Technical aspects and development of transcatheter aortic valve implantation," *Journal of Cardiovascular Development and Disease*, vol. 9, no. 8, p. 282, 2022.

[18] F. Nappi, S. S. Avtaar Singh, P. Nappi, and A. Fiore, "Biomechanics of transcatheter aortic valve implant," *Bioengineering*, vol. 9, no. 7, p. 299, 2022.

[19] E. S. Fioretta, S. E. Motta, V. Lintas, S. Loerakker, K. K. Parker, F. P. Baaijens, V. Falk, S. P. Hoerstrup, and M. Y. Emmert, "Next-generation tissue-engineered heart valves with repair, remodelling and regeneration capacity," *Nature Reviews Cardiology*, vol. 18, no. 2, pp. 92–116, 2021.

[20] S. B. Anam, B. J. Kovarovic, R. P. Ghosh, M. Bianchi, A. Hamdan, R. Haj-Ali, and D. Bluestein, "Validating in silico and in vitro patient-specific structural and flow models with transcatheter bicuspid aortic

valve replacement procedure," *Cardiovascular Engineering and Technology*, pp. 1–17, 2022.

[21] S. Pfensig, S. Kaule, R. Ott, C. Wüstenhagen, M. Stiehm, J. Keiler, A. Wree, N. Grabow, K.-P. Schmitz, and S. Siewert, "Numerical simulation of a transcatheter aortic heart valve under application-related loading," *Current Directions in Biomedical Engineering*, vol. 4, no. 1, pp. 185–189, 2018.

[22] J. A. Brown, J. H. Lee, M. A. Smith, D. R. Wells, A. Barrett, C. Puelz, J. P. Vavalle, and B. E. Griffith, "Patient–specific immersed finite element–difference model of transcatheter aortic valve replacement," *Annals of Biomedical Engineering*, vol. 51, no. 1, pp. 103–116, 2023.

[23] R. Plitman Mayo, H. Yaakobovich, A. Finkelstein, S. C. Shadden, and G. Marom, "Numerical models for assessing the risk of leaflet thrombosis post-transcatheter aortic valve-in-valve implantation," *Royal Society open science*, vol. 7, no. 12, p. 201838, 2020.

[24] X. Liu, W. Zhang, P. Ye, Q. Luo, and Z. Chang, "Fluid-structure interaction analysis on the influence of the aortic valve stent leaflet structure in hemodynamics," *Frontiers in Physiology*, p. 910, 2022.

[25] S. Reza, M. Bianchi, B. Kovarovic, S. Anam, M. J. Slepian, A. Hamdan, R. Haj-Ali, and D. Bluestein, "A computational framework for post-tavr cardiac conduction abnormality (cca) risk assessment in patient-specific anatomy," *Artificial Organs*, vol. 46, no. 7, pp. 1305–1317, 2022.

[26] M. Peirlinck, F. S. Costabal, J. Yao, J. Guccione, S. Tripathy, Y. Wang, D. Ozturk, P. Segars, T. Morrison, S. Levine *et al.*, "Precision medicine in human heart modeling: Perspectives, challenges, and opportunities," *Biomechanics and modeling in mechanobiology*, vol. 20, pp. 803–831, 2021.

[27] L. Sörnmo and P. Laguna, *Bioelectrical signal processing in cardiac and neurological applications*. Academic press, 2005, vol. 8.

[28] J. R. Pinto, J. S. Cardoso, A. Lourenço, and C. Carreiras, "Towards a continuous biometric system based on ecg signals acquired on the steering wheel," *Sensors*, vol. 17, no. 10, p. 2228, 2017.

[29] J. R. Pinto, J. S. Cardoso, and A. Lourenço, "Evolution, current challenges, and future possibilities in ecg biometrics," *IEEE Access*, vol. 6, pp. 34 746–34 776, 2018.

[30] S. Miao, R. Liao, and Y. Zheng, "A hybrid method for 2-d/3-d registration between 3-d volumes and 2-d angiography for trans-catheter aortic valve implantation (tavi)," in *2011 IEEE International Symposium on Biomedical Imaging: From Nano to Macro*. IEEE, 2011, pp. 1215–1218.

[31] B. Mildenhall, P. P. Srinivasan, M. Tancik, J. T. Barron, R. Ramamoorthi, and R. Ng, "Nerf: Representing scenes as neural radiance fields for view synthesis," *Communications of the ACM*, vol. 65, no. 1, pp. 99–106, 2021.

[32] J. L. Schonberger and J.-M. Frahm, "Structure-from-motion revisited," in *Proceedings of the IEEE conference on computer vision and pattern recognition*, 2016, pp. 4104–4113.

[33] C. Griwodz, S. Gasparini, L. Calvet, P. Gurdjos, F. Castan, B. Maujean, G. De Lillo, and Y. Lanthony, "Alicevision meshroom: An open-source 3d reconstruction pipeline," in *Proceedings of the 12th ACM Multimedia Systems Conference*, 2021, pp. 241–247.

APPENDIX A
THV DEVICE GEOMETRY VISUALIZATION FOR VALIDATED TARGETS

This section showcases the results of the computational framework introduced in the study through a comprehensive display of evaluated targets. It provides an in-depth look of THV device geometries generated by the framework for each analysed target.

To ensure a thorough evaluation, a systematic methodology was used in selecting the target models. The selection process involved evenly dividing the data into five frames, with each column of the figures representing a time series state t_i. The number of sequences and frames for each patient may vary. The 17 patients are designated using capital letters (A, B, C) and each row represents a sequence, indicated by the patient identifier combined with a number (e.g., A1, A2). The results are displayed in a bold style to emphasize the best performance of the metric, with the worst performance further highlighted in red for improved visual emphasis. The sequences were treated independently from each other for analysis purposes.

The results displayed in the gallery play a crucial role in reinforcing the conclusions and findings of the study, offering valuable insight into the limitations and potential applications of the framework.

Time-series

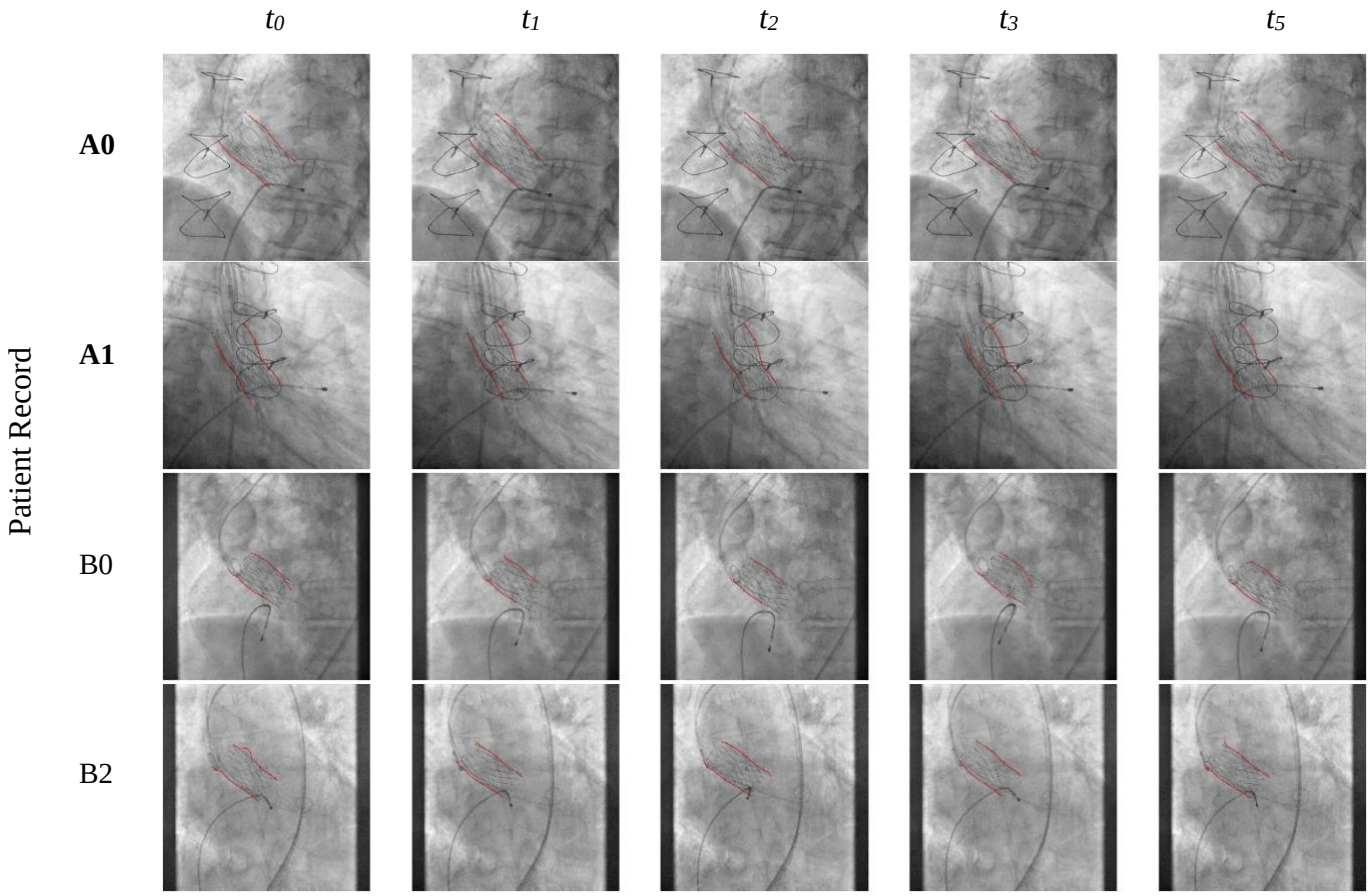

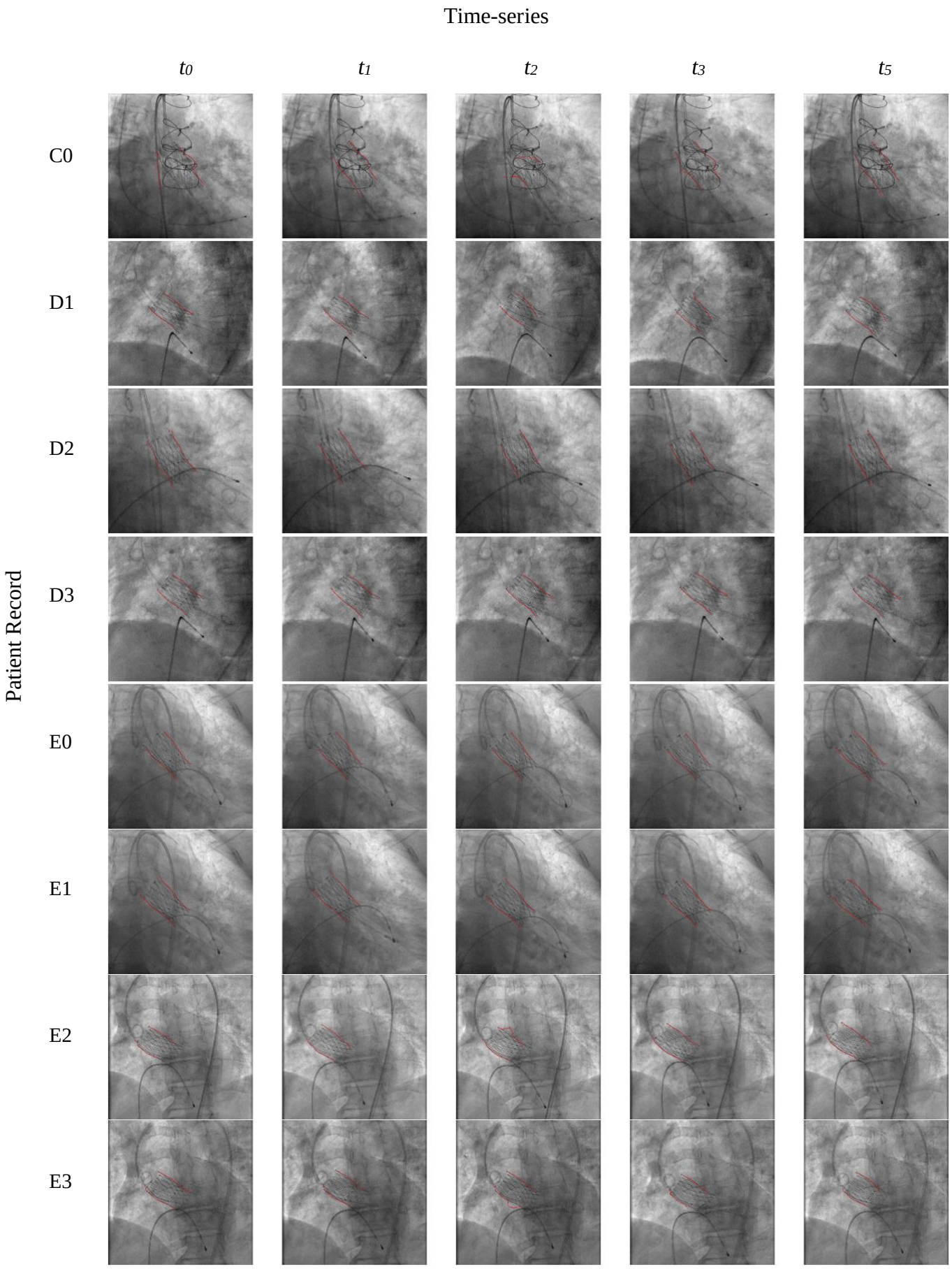
Time-series
t_0
t_1
t_2
t_3
t_5
Patient Record
C0
D1
D2
D3
E0
E1
E2
E3

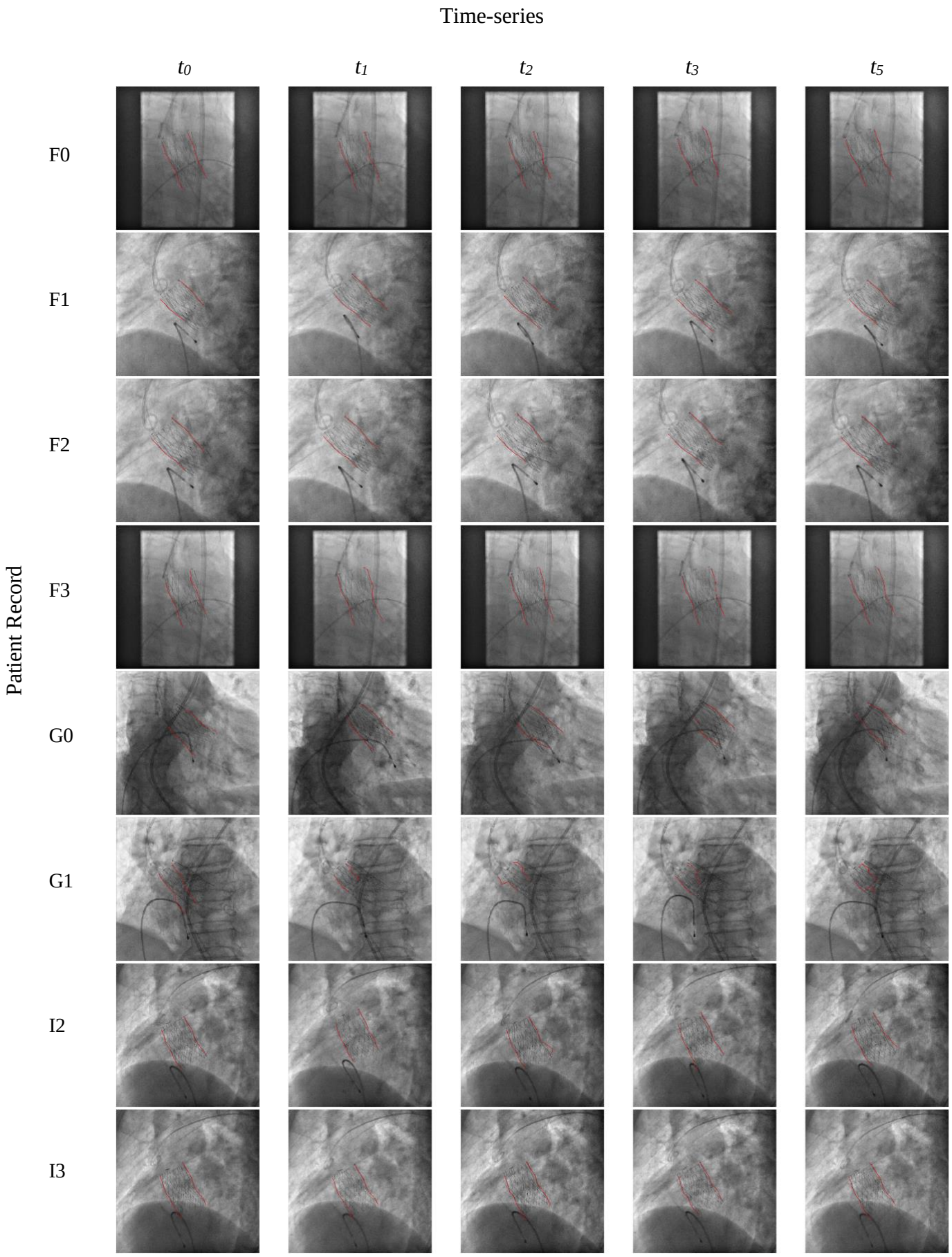
Time-series
t_0
t_1
t_2
t_3
t_5
Patient Record
F0
F1
F2
F3
G0
G1
I2
I3

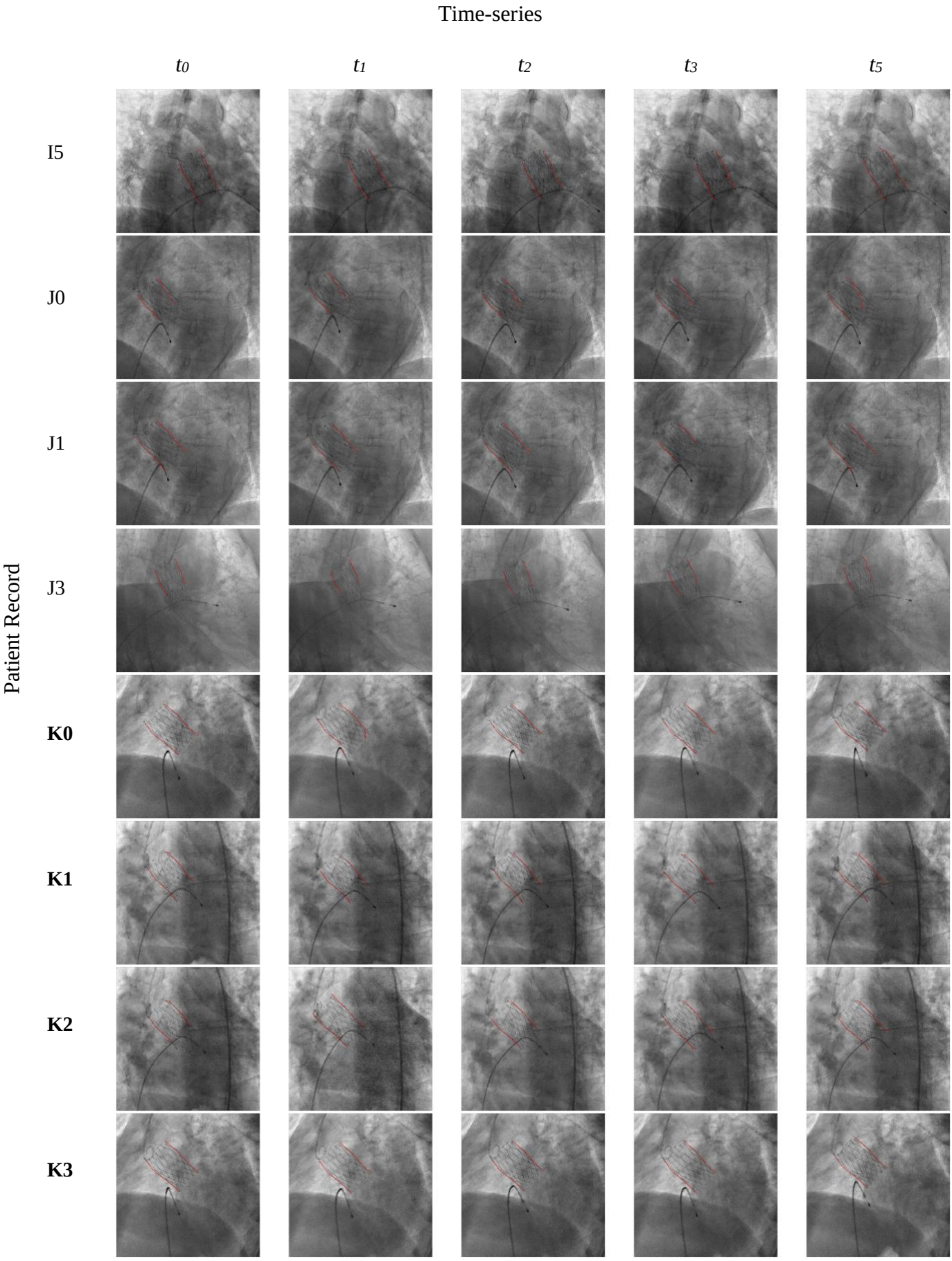
Time-series
t_0
t_1
t_2
t_3
t_5
Patient Record
I5
J0
J1
J3
K0
K1
K2
K3

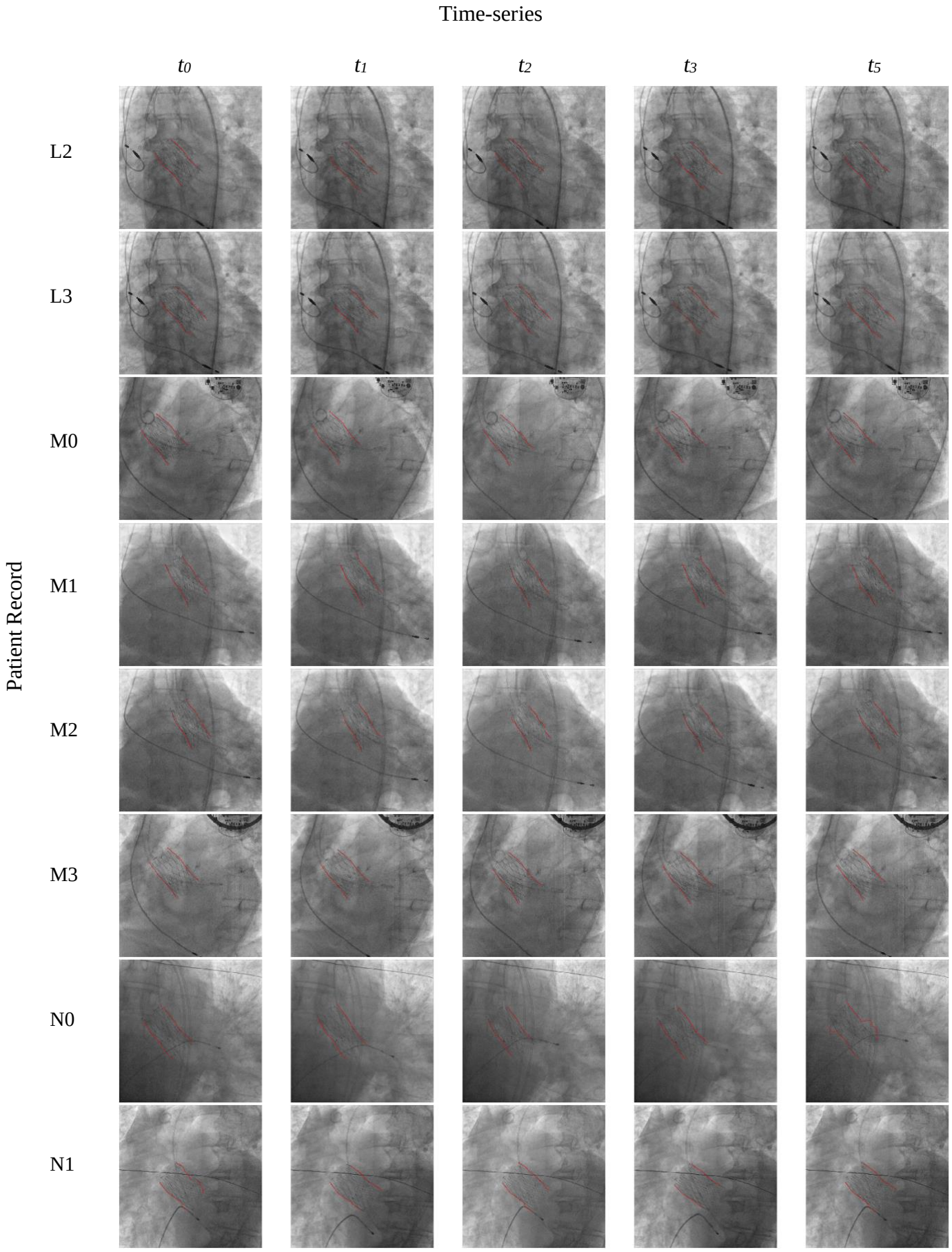
Time-series
t_0
t_1
t_2
t_3
t_5
Patient Record
L2
L3
M0
M1
M2
M3
N0
N1

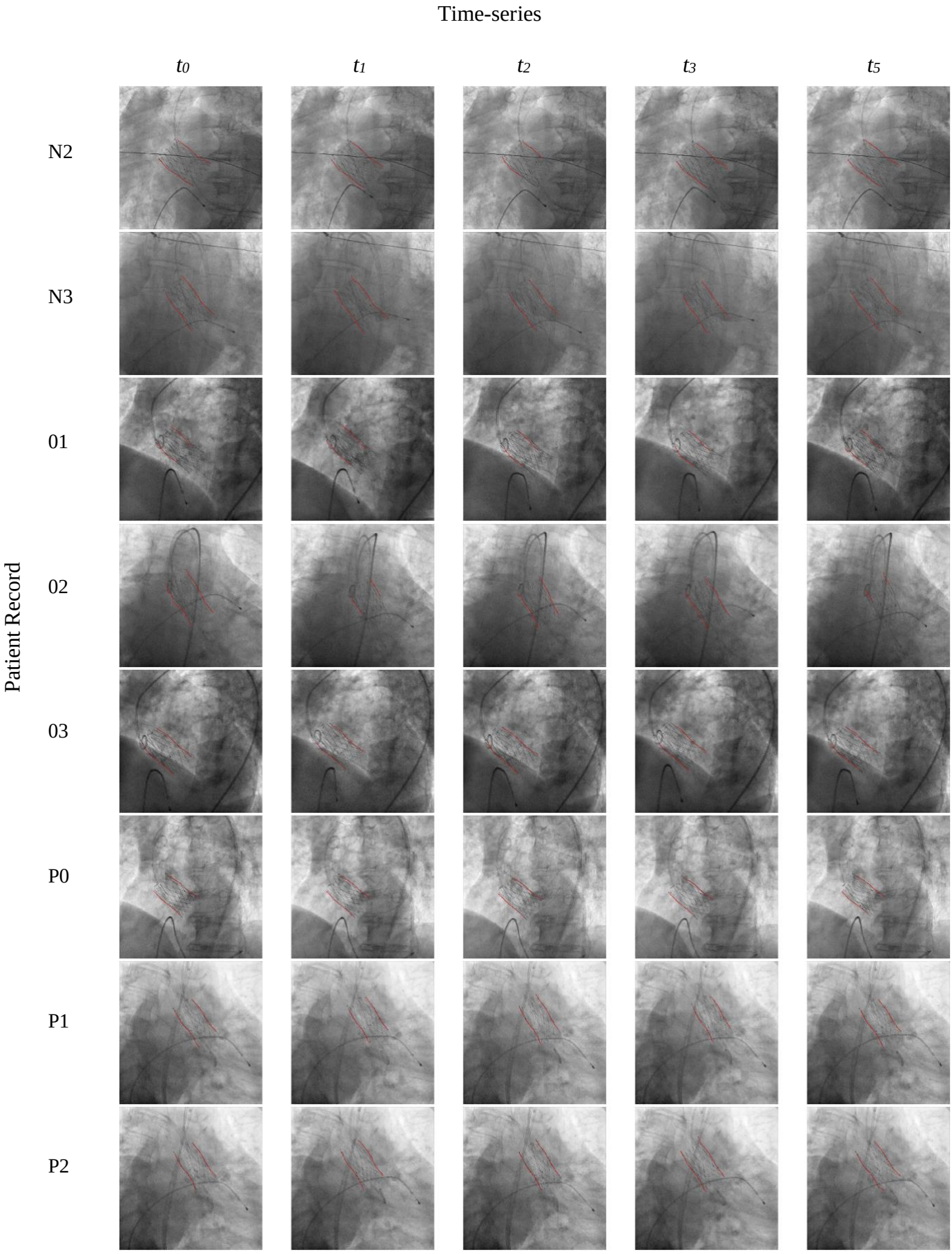
Time-series
t_0
t_1
t_2
t_3
t_5
Patient Record
N2
N3
01
02
03
P0
P1
P2

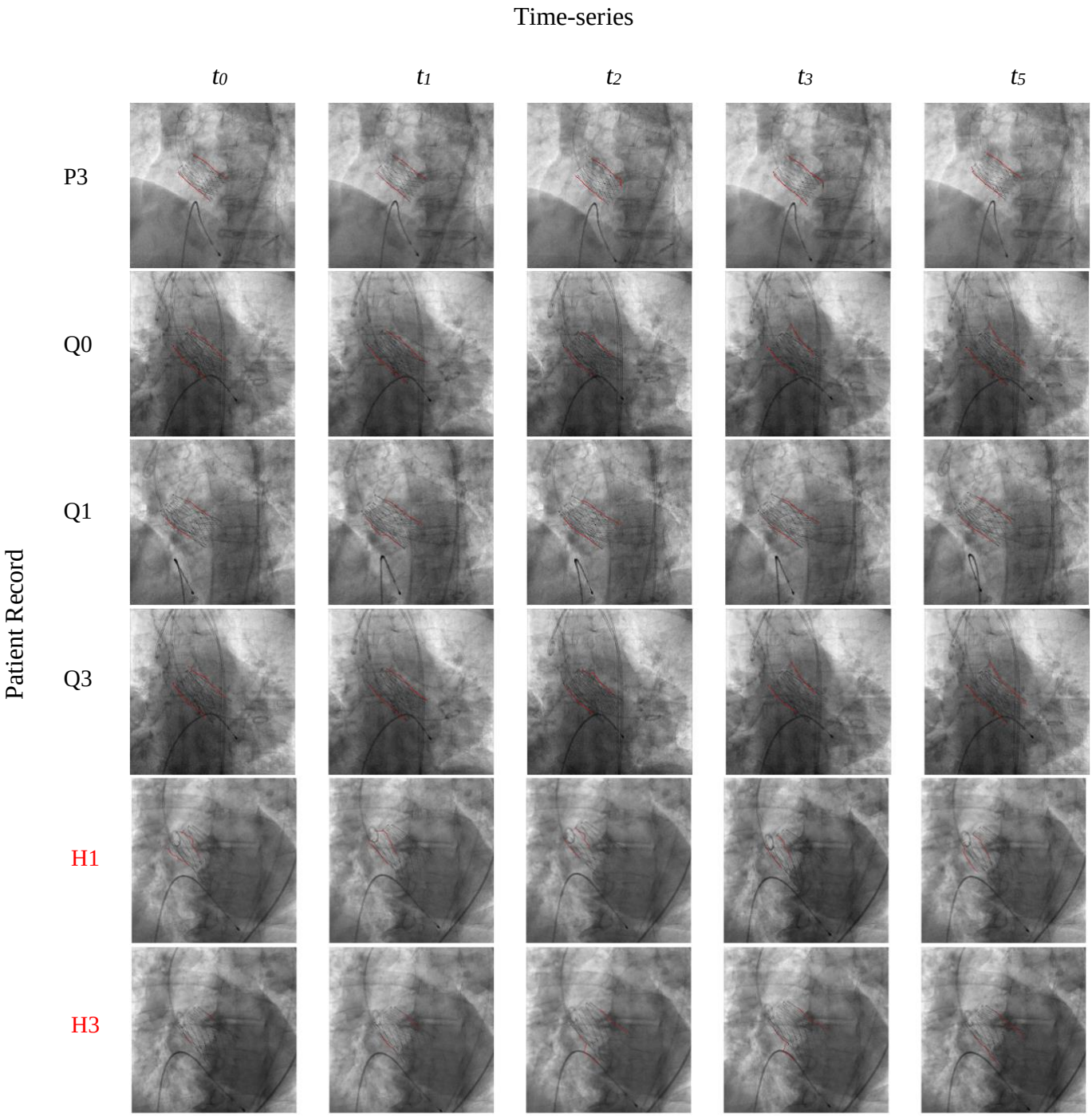
Time-series
t_0
t_1
t_2
t_3
t_5
Patient Record
P3
Q0
Q1
Q3
H1
H3